Vol 17 No 6, June 2008
1674-1056/2008/17(06)/2010-08

Chinese Physics B

© 2008 Chin. Phys. Soc.
and IOP Publishing Ltd

Radiation-induced resistance oscillation and instability in GaAS/AlGaAS heterostructure under transverse magnetic fields*

Yang Gui(杨 癸)[a)†], Tu Bi-Hong(涂必红)[a)], Li Guo-Hui(李国辉)[b)]
Zhao Hong-Wei(赵宏伟)[a)], and Zhou Shi-Ping(周世平)[a)]

[a)] *Department of Physics, Shanghai University, Shanghai* 200444, *China*

[b)] *Department of Communication Engineering, Shanghai University, Shanghai* 200072, *China*

(Received 19 March 2007; revised manuscript received 15 October 2007)

This paper studies dynamics of a modulation-doped GaAs/AlGaAs heterostructure under transverse magnetic fields and microwave radiations. It finds that negative differential conductivity, due to the real-space electron transfer and delayed dielectric relaxation of the interface potential barrier, can lead to complex behaviours when a relatively small magnetic field is applied. Quasiperiodicity, frequency-locking and the routes from period-doubling to chaos are found. Under a large magnetic field, however, two time-independent homogeneous steady states exist; and the longitudinal resistance of the system shows an interesting oscillation with period tuned by the ratio of microwave radiation frequency ω to the cyclotron frequency ω_c and local minima at $\omega/\omega_c = \text{integer} + 1/4$.

Keywords: heterostructure, chaos, bifurcation, resistance oscillation
PACC: 0547, 7220H, 7340L

1. Introduction

In the last two decades, especially since the discovery of the quantum Hall effect[1] a lot of progress has been made in the study of two-dimensional electron systems (2DES) theoretically[2−4] and experimentally.[5] The central motivation has been the possible applications of these systems in the devices.[6] It has been shown that the n-GaAs and a number of other compound semiconductors with negative differential conductivity (NDC) can exhibit many interesting nonlinear effects, such as a hysteresis loop in the current–voltage curve,[7] self-sustained oscillations and chaos[8−10] when these systems are subjected to external electric and magnetic fields.[4,5,7−10] In 1994, Aoki *et al*[5] found the route from period-doubling to chaos when the system was connected with the application of an ac-modulated bias voltage. Recently, Tzeng *et al*[7] used the two-impurity-level model to research into the dynamics of a n-GaAs semiconductor. The main feature is that the system undergoes a series of period-doubling bifurcation to chaos when the magnetic field varied between (0.1–0.2) Teslas that is at small Hall angles calculated from $\tan\theta = \mu B$.

Surprisingly, Mani used ultrahigh-mobility GaAS/Al_xGa_{1-x}AS sample and observed a new physical phenomenon: the zero-resistance states (ZRS) at low temperature less than 6 K and resistance oscillations when these systems were under the influence of a moderate magnetic field B and microwave(MW) radiations.[11] It has been shown that the radiation-induced resistance oscillation period is controlled by the ratio of the radiation frequency ω to the cyclotron frequency $\omega_c = eB/m^*$ of the 2DES (m^* is the effective mass) and the vanishing longitudinal resistance occurred at near ω/ω_c=integer+1/4. This striking discovery of resistance oscillations has been experimentally proved by different groups.[12−18] Subsequently, a number of theoretical models[19−25] have been proposed to understand the origin of the MW-induced resistance oscillation. Most models suggest that the oscillation is related to the instability of the system that occurs due to the existence of the NDC region.[26−29] From the assumed resistivity-current relation of $\rho_d(j^2)$, Andreev *et al*[27] pointed out a negative linear response conductance implies that the ZRS is intrinsically unstable: the system spontaneously developed a nonvanishing local current density, which

*Project supported by the National Natural Science Foundation of China (Grant No 60371033).
†E-mail: kuiziyang@graduate.shu.edu.cn

almost everywhere had a specific magnitude j_0 determined by the condition that the component of electric field parallel to the local current vanishes. The existence of this instability is then to imply the observed ZRS and resistance oscillations when the fluctuation such as a MW irradiation presents. We will show that a positive resistance oscillation is expected when the system was properly biased within the NDC region under a MW radiation at very high temperatures (the room temperature) as Andreev and co-workers[27] argued.

In this paper, we investigate dynamics of the modulation-doped GaAS/Al_xGa_{1-x}AS heterostructure under transverse magnetic fields and MW radiations at room temperature. We propose a mechanism that underlies the NDC response based on real-space transfer of electrons between the GaAs layer and the doped AlGaAS layer. Comparing with our previous work Ref.[8], we consider the magnetic field effects on the system. The analysis shows that the stability of the system and the NDC region in current–voltage $I(v)$ characteristics will be modified by a crossed magnetic field B. For low magnetic fields ($B \leq 0.5$ T, which means a negligible Hall angle), self-sustained oscillations and bifurcation between oscillationary and stationary states are predicted as the system biased within the NDC region. These results are similar to Ref.[8] except that MW radiation induced bifurcations from periodic to chaotic state have been clearly generated which agrees with the experimental observations.[5] However, in the case of a sufficient large B, there exist only two almost time-independent states as those shown in Ref.[27]. An oscillation is then followed when the system is switched between the two steady states by a MW irradiation. Indeed, varying the frequency of the MW irradiation, we find that the positive resistance oscillations are periodic with local minima at ω/ω_c=integer+1/4. Our numerical simulations are in agreement with the theoretical prediction in Ref.[27].

2. Model

In this section, we give a brief introduction to the model. Figure 1 shows the energy-band diagram of a modulation-doped GaAS/Al_xGa_{1-x}AS heterostructure. L_1 and L_2 are the width of GaAs and AlGaAs. The GaAs layer is undoped, while the AlGaAs layer is heavily n-doped with the donor density N_D. ΔE_c is the conduction band discontinuity. ϕ_b represents the interface potential barrier. μ_1 and μ_2 are the mobility of the electrons at zero magnetic field in the GaAs and AlGaAs layer, respectively. Figure 2 is the circuit diagram of the AC biased heterostructure under a transverse magnetic field B and MW radiations.

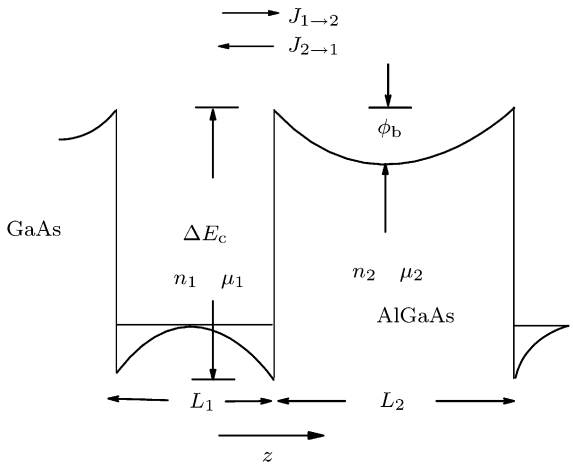


Fig.1. The energy-band diagram of GaAs/AlGaAs.

The origin of the NDC can be qualitatively understood as follows. As the bias U increases, the electrons in GaAs layer will get enough kinetic energy which is higher than ΔE_c to tunnel across the barrier into the AlGaAs layer, which is similar to a thermionic emission from the GaAS layer into the doped AlGaAs layer. This makes an increase of carrier density in the AlGaAs channel which has several consequences. First, since the mobility in the AlGaAs layer is much lower than that in the undoped GaAs layer, an increase of the carrier density implies also somewhat decrease in the longitudinal current density, that is, a NDC. Second, the potential barrier ϕ_b will decrease with some delay due to the finite dielectric relaxation time, which leads then to an increase of backward current with some reduction of the carrier density in the AlGaAs, which, in turn, depresses the backward thermionic emission current, forming complete cycles of real-space charge transfer.[30] Complex dynamic behaviours are expected, accordingly.

We choose the carrier density n_1 in the GaAs layer, the interface barrier ϕ_b and the in-plane electric field components E_x and E_y as variables in our model. From the current continuity equation $\nabla \cdot J + \partial n/\partial t = 0$, we obtain

$$\frac{\mathrm{d}n_1}{\mathrm{d}t} = \frac{J_{1\to2} - J_{2\to1}}{eL_1}, \tag{1}$$

where

$$J_{1\to 2} = -en_1\sqrt{\frac{E_1}{3\pi m_1^*}}\exp\Big(-\frac{3\Delta E_{\rm c}}{2E_1}\Big),$$
$$J_{2\to 1} = -en_2\sqrt{\frac{E_2}{3\pi m_2^*}}\exp\Big(-\frac{3\phi_{\rm b}}{2E_2}\Big),$$

$J_{1\to 2}$ ($J_{2\to 1}$) are the thermionic emission current densities from GaAs to AlGaAs (AlGaAs→ GaAs) layer. The spatially averaged carrier density in the GaAS and AlGaAs layers are, respectively, defined as $n_1 = (1/L_1)\int_{-L_1}^{0} n(z,t){\rm d}z$ and $n_2 = (1/L_2)\int_{0}^{L_2} n(z,t){\rm d}z$. For the conservation of the total number of carriers, we have

$$n_1L_1 + n_2L_2 = N_{\rm D}L_2. \tag{2}$$

Here m_i^* (i=1, 2) are electron effective masses in GaAS and AlGaAs layers. The mean energy as a function of the applied electric field E_x is roughly estimated by $E_i \approx E_{\rm L} + \tau_E e\mu_i E_x^2$ with τ_E the energy relaxation time. $E_{\rm L} = (3/2)k_{\rm B}T_{\rm L}$ is the mean carrier energies, and $T_{\rm L}$ is the lattice temperature. The thermionic-emission current corresponds to the following physical picture. Electrons in GaAs layer with the energy less than $\Delta E_{\rm c}$ cannot propagate to the doped AlGaAs layer; whereas those with energies larger than $\Delta E_{\rm c}$ will emit across the barrier without collisions. This is correct when L_1 is smaller than the mean free path of electrons.

As for the formation of the $\phi_{\rm b}$, an important feature is the ubiquitous presence of space charges.[31] According to the Poisson's equation, the space charge induces a further feedback between the charge-carrier distribution and the electric potential distribution governing the transport. This mutual nonlinear interdependence is particularly pronounced in the case of semiconductor heterostructures and low-dimensional structures, in which abrupt junctions between different materials on an atomic length scale cause conduction band discontinuities resulting in potential barriers. The interface barrier $\phi_{\rm b}$ is governed by the space-charge dynamics in the AlGaAs layer and the resulting internal electric field. The dynamics of $\phi_{\rm b}$[30] is given by

$$\dot{\phi_{\rm b}} = \frac{e}{\varepsilon}\Big[-\mu_2 N_{\rm D}\phi_{\rm b} + \mu_2\frac{e^2}{2\varepsilon}L_1^2n_1^2 - eL_1L_2\dot{n_1}\Big]. \tag{3}$$

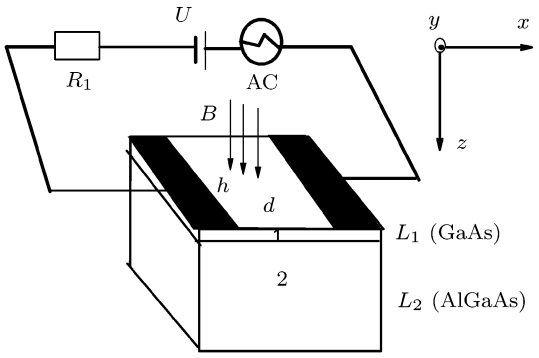


Fig.2. The circuit diagram of GaAs/AlGaAS with lateral dimensions h, d.

Choosing the coordinate system such that the electric field $\boldsymbol{E} = \hat{E}_x + \hat{E}_y$ and a static magnetic field in the Z direction $\boldsymbol{B} = B\hat{Z}$, we obtain the dynamic equations for the electric field:[32]

$$\varepsilon\dot{E}_x = \sigma_{\rm l}(E_x - E_0) + \sigma_{\rm m}E_x + \sigma_{\rm n}E_y, \tag{4}$$
$$\varepsilon\dot{E}_y = \sigma_{\rm m}E_y + \sigma_{\rm n}E_x, \tag{5}$$

where

$$\sigma_{\rm l} = -d/[h(L_1+L_2)R_{\rm l}],$$
$$\sigma_{\rm m} = -(en_1\mu_{1\rm B}L_1 + en_2\mu_{2\rm B}L_2)/(L_1+L_2),$$
$$\sigma_{\rm n} = -eB(n_1\mu_{1\rm B}\mu_1L_1 + n_2\mu_{2\rm B}\mu_2L_2)/(L_1+L_2),$$
$$\mu_{i\rm B} = \mu_i/(1+\mu_i^2B^2)\quad (i=1,2),$$

ε is the permittivity and E_0 is the applied field. In our numerical simulations we use the dimensionless variables: $Y_1 = n_1/N_{\rm D}$, $Y_2 = \mu_1E_x/V_{\rm ds}$, $Y_3 = \mu_1E_y/V_{\rm ds}$, $Y_4 = \phi_{\rm b}/(k_{\rm B}T_{\rm L})$, $T = t/\tau_E$.

In this model, we have neglected the diffusive contributions that has to be included only when the GaAs/AlGaAs layer-thickness is much larger than the mean free path of the electrons. Intervalley transfer has been shown[33] to be negligible in comparison with real-space transfer when the electric field is in the range of $E_x \le 5.0$(kV/cm), as used in the research. Quantum effects like the quantum-transmission coefficient or tunnelling through the barrier are also ignored.[34] In addition, quantum size effects are neglected since the current–voltage characteristic is almost independent on the quasi-two-dimensional subbands below the barrier when the layer thickness is greater than 10 nm.

Table 1. The parameter values used in this paper.

N_D/cm^{-3}	10^{17}	L_1/nm	10
$\mu_1/(cm^2/Vs)$	8000	L_2/nm	20
$\mu_2/(cm^2/Vs)$	50	T_L/K	300
ΔE_c/meV	250	m_1^*/m_0	0.067
h/mm	1	m_2^*/m_0	$(0.067 + 0.083 \times 0.3)$
τ_E/s	5.0×10^{-12}	d/μm	50
$\varepsilon/\varepsilon_0$	12	m_0/kg	0.91×10^{-30}
ε_0/Fm^{-1}	8.854×10^{-12}	R_l/Ω	1144
k_B/JK^{-1}	1.380×10^{23}	V_{ds}/ms^{-1}	5.0×10^7

3. Simulation and numerical results

3.1. NDC associated complex dynamical behaviours at low magnetic fields

In this section, we present the numerical results for model Eqs.(1)–(5) by using the parameter values in Table 1.[35] The fourth order Runge–Kutta technique is used. The transport properties of a semiconductor heterostructure show up most directly in its current–voltage characteristic under time-independent bias conditions. For the case of a DC bias voltage, we find that the static current–voltage curve exhibits an inverted S-shaped NDC (SNDC) feature when the bias is in a certain range(see below) that expands as the magnetic field increases. We first study the equilibrium points of the dynamic equations (1), (3)–(5) by setting time derivatives in the left-hand side of these equations to zero. Figure 3(a) shows the static current-density $j_x = eE_x(n_1\mu_{1B}L_1 + n_2\mu_{2B}L_2)/(L_1 + L_2)$ versus the drift electric field E_x at B=0.3 T. As the control parameter U increases, the load-line (the bold straight line) shifts in parallel along the direction shown by the arrow in the figure. The load-line becomes tangential to the characteristic curve at U_1 or U_2 , which set boundaries for the NDC response as $U_1 < U < U_2$. The diagram of the current I_x versus the control parameter U is plotted in Fig.3(b). Clearly, an inverted SNDC region of range getting wider is indicated by the solid, dash, dot and dash-dot lines for B=0, 0.3, 2 and 3 T, respectively. Complex dynamic behaviours are then expected due to the instability of the SNDC region when there are perturbations such as MW irradiations.

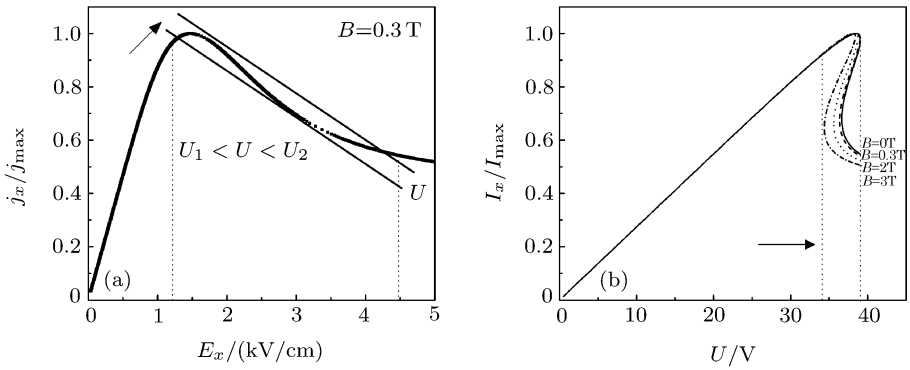


Fig.3. (a) The static normalized current-density j_x versus the drift electric field E_x. The load line is shown for different intersection points. (b) The normalized current I_x as a function of the control parameter U. The current exhibits inverted SNDC in the region of $U_1 < U < U_2$.

Then, we study dynamical behaviours of the $GaAs/Al_xGa_{1-x}As$ heterostructure under relatively low magnetic fields B and MW radiations. We find that the dynamic behaviours are similar when B varies in the range of (0, 0.5) T. We discussed the case for B=0.3T. The nature of the stability of a steady state (a fixed point in the phase space) is determined by the eigenvalues of the system's Jacobian matrix. There

are four eigenvalues for a 4-dimensional dynamic system. Note added: the real part of the first eigenvalue ($\mathrm{Re}(\lambda_1)$) is always negative and hasn't been shown in Fig.4 while the others ($\mathrm{Re}(\lambda_i)$, i=2, 3, 4) are negative or positive at different fixed points. We are interested in the case that some $\mathrm{Re}(\lambda)$ is positive because the nonlinear oscillations of the electron density and the potential barrier can be found. Figure 4 shows the real parts of the eigenvalues as a function of the static drift electric field E_x. The inset is to make the interested image clearly. From Fig.4 one can discuss bifurcations of the steady states in the phase space. With increasing E_x, a stable node turns to a stable focus, which becomes unstable when $E_x > E_1$. The unstable focus is then transformed into a saddle point and vanishes at E_{11}. Similar bifurcation scenario occurs when E_x varies within (E_{21}, E_2).

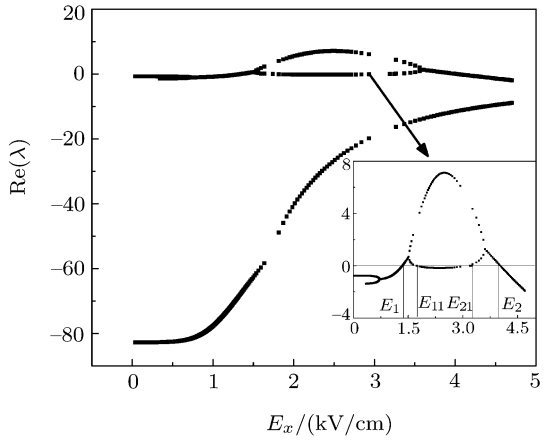


Fig.4. The real parts of the eigenvalue as a function of the drift electric field E_x.

A complete bifurcation diagram obtained by solving Eqs.(1)–(5) dynamically is shown in Fig.5. The bold lines represent the stable states. The thin and the dashed lines denote unstable focus and saddle-points, respectively. As the electric field E_0 increases to $E_{\mathrm{a1}}(2)$, a stable and an unstable limit cycle are generated. The unstable limit cycle intersects with the saddle point at $E_{\mathrm{a2}}(3)$, and forming then a saddle(3)-to-saddle(4) homoclinic orbit around the fixed points. With further increasing E_0, another unstable limit cycle appears at (4) and disappears at $E_{\mathrm{a3}}(5)$ through the Hopf bifurcation. When $E > E_{\mathrm{a4}}(6)$, an unstable limit cycle is generated and it intersects with the saddle point at $E_{\mathrm{a5}}(7)$ accompanied with the saddle(7)-to-saddle(8) homoclinic orbit. The unstable limit cycle from the bifurcation of (8) intersects with the stable limit cycle at $E_{\mathrm{a6}}(9)$. For $E > E_{\mathrm{a6}}(9)$, the stable focus is expected. The stable limit cycle (slc) is a sign of the self-sustained oscillations whose resonant frequency f_0 is found to be f_0=90.744 GHz (not shown).

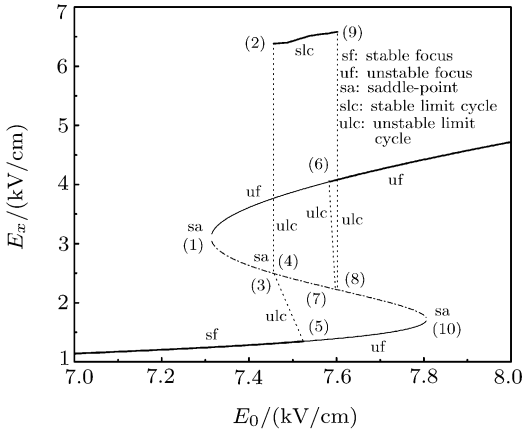


Fig.5. The bifurcation diagram of the static electric field E_x with the control parameter $E_0 = U/d$.

From Fig.5, we can find that there coexist two attractors (the stable limit cycle and the stable focus) when $E_{\mathrm{a2}}(3) < E_0 < E_{\mathrm{a3}}(5)$ or $E_{\mathrm{a5}}(7) < E_0 < E_{\mathrm{a6}}(9)$. We present the projection of the phase portrait in (n_1, ϕ_{b}) plane for $E_{\mathrm{a2}}(3) < E_0 < E_{\mathrm{a3}}(5)$ in Fig.6, which shows the coexistence of the two attractors. Consequently, the dynamic behaviours can be essentially attributed to the real-space transfer of carriers.

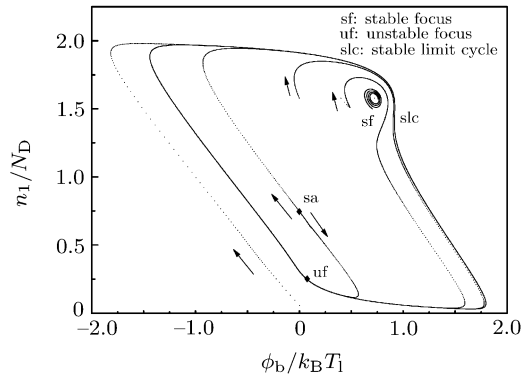


Fig.6. Coexistence of two stable attractors. Phase portraits in the (n_1, ϕ_{b}) plane. The control parameter is within $E_{\mathrm{a2}}(3) < E_0 < E_{\mathrm{a3}}(5)$ (E_0=7.5 kV/cm). The conduction electron concentration n_1 is in units of N_{D} and ϕ_{b} is in units of $k_{\mathrm{B}}T_{\mathrm{l}}$.

We now study system states varying with the MW radiation that is physically mapped onto an AC bias, that is, the total bias is written as $U = U_0(1 + A\sin(2\pi n f_0 t))$. For B=0.3T, the NDC region is between 36.3 V< U <39.4 V (See Fig.3). We choose U_0=37.5 V, n=9.5 and the relative amplitude $0 \le A \le 0.8$. Such a choice can cover the physically interesting region completely. We use the Poincaré

map technique to specify the states of the system. The Poincaré map orbit is plotted by sampling the trajectory every $T = 1/f_0$ seconds onto the (n_1, E_x) plane. As the relative amplitude varies in the range of $0 \leq A \leq 0.0697$, only period one limit cycle exists, corresponding to a fixed point in the Poincaré section. As the relative amplitude increases from 0.0697 to 0.0774, period two oscillations present(two fixed points). For $0.0774 < A \leq 0.07874$, period-four and period-eight oscillations appeared successively. With further increasing the amplitude A to 0.08, the oscillations become nonperiodic and random-like. This is

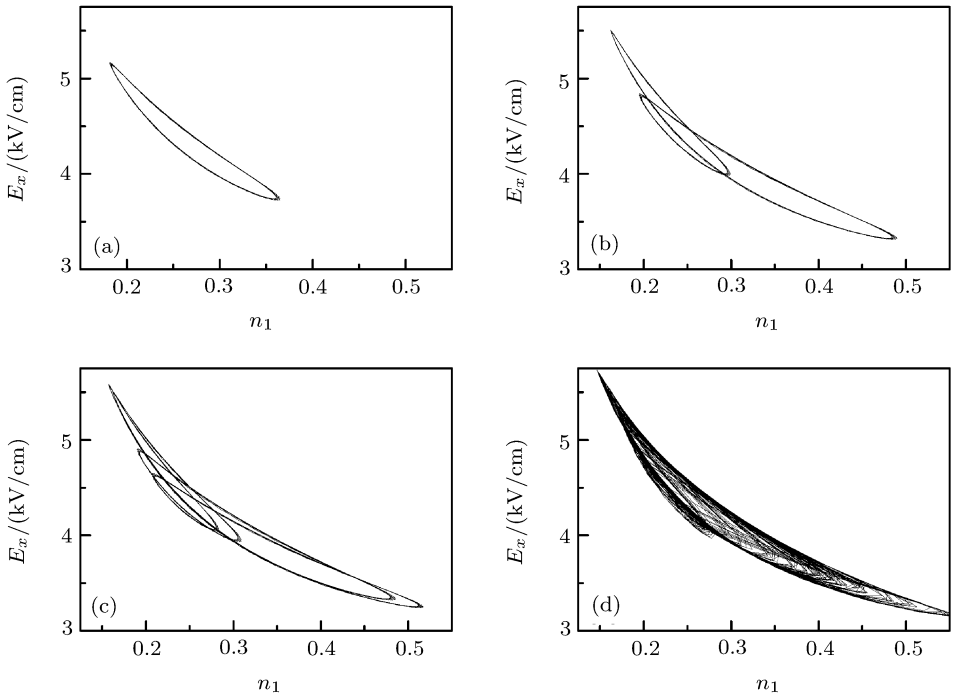


Fig.7. The projection of the phase portrait in the (n_1, E_x) plane, and the amplitude A has the value (a) 0.064 (a limit cycle), (b) 0.076 (period-2 oscillation), (c) 0.078 (period-4 oscillation), (d) 0.08 (chaos). n_1 is in units of $N_{\rm D}$.

a sign of chaos, and a good indication of the routes from period-doubling to chaos with the MW amplitude. Figures 7(a)–7(d) show the projection of the phase portrait in the (n_1, E_x) plane for period 1, period 2, period 4, and chaotic states at different relative amplitude values. To make the process of the routes from period-doubling to chaos clearly, we give the bifurcation diagram of the drift electric field E_x versus the relative amplitude A in Fig.8. Similar behaviours are found when A varies with 0.08–0.8. Therefore, we can draw a conclusion that the instability of the NDC would lead to self-sustained oscillation, frequency-locking and unpredicted or chaotic states when the Hall angle is very small, or the magnetic field intensity is weak.

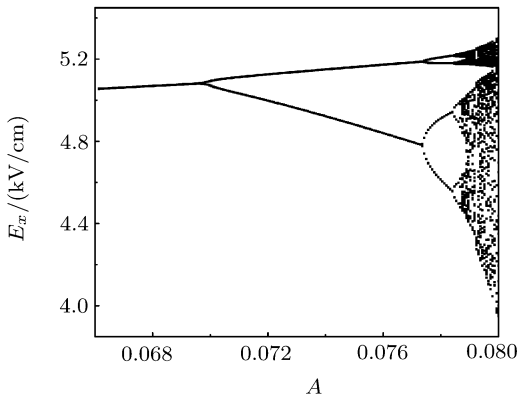


Fig.8. The bifurcation diagram of the drift electric field E_x versus the amplitude A. For different A, the dynamical behaviour of the system is different. It clearly shows the route from period-doubling to chaos.

3.2. Time-independent states and positive resistance state oscillation with MW illumination at high fields

For the magnetic field B=3.0 T so as to yield a large Hall angle (∼67.5 degrees calculated from $\tan\theta = \mu B$), the static current–voltage curve exhibits also an inverted SNDC. However, the instability of the system changes dramatically due to a strong Lorentz force sensed by the carriers. Instability analysis shows that it behaves as a bistable system. Biased within the SNDC region, the system falls into a steady state thereinto. Transitions between the two steady states will be induced by MW irradiations. Corresponding to this, a constant stable positive resistance state can be shown through the time average with the period of the MW irradiation.

Rewrite $U = U_0(1 + A\sin\omega t)$ where ω is the angular frequency of the MW irradiation. We choose U_0=36.25 V and the relative amplitude A=0.05, so that the heterostructure operates in the NDC region. The current–voltage curve is plotted in Fig.9(a). Indeed, there presents only two nearly time-independent stable steady states, similar to the degenerate states 'j_0' and '$-j_0$' suggested by Andreev *et al.*[27] Furthermore, the bistable states remain invariant under the MW irradiations, and the system is switched between these states with a period which precisely equals to that of the MW illumination. This is shown by the plot of the longitudinal resistance versus the time, as the inset of Fig.9(a). Where the resistance is calculated from $R_{xx} = U_x/I_x$ with $U_x = E_x d$ the voltage over the sample and $I_x = (E_0 - E_x)d/R_l$ the current. Its time average is then a positive value, implying that the system is in a positive resistance state as suggested by Andreev *et al.*[27] Interestingly, the average longitudinal resistance oscillates with MW radiation frequencies, as shown in Fig.9(b). In addition, we change the amplitude of MW illumination. The short dash, solid and short dot lines correspond to the data for A=0.02, 0.05 and 0.08, respectively. Clearly and remarkably, the results show that the oscillations are periodic and the local minima of the resistance located at or very close to ω/ω_c=integer+1/4.

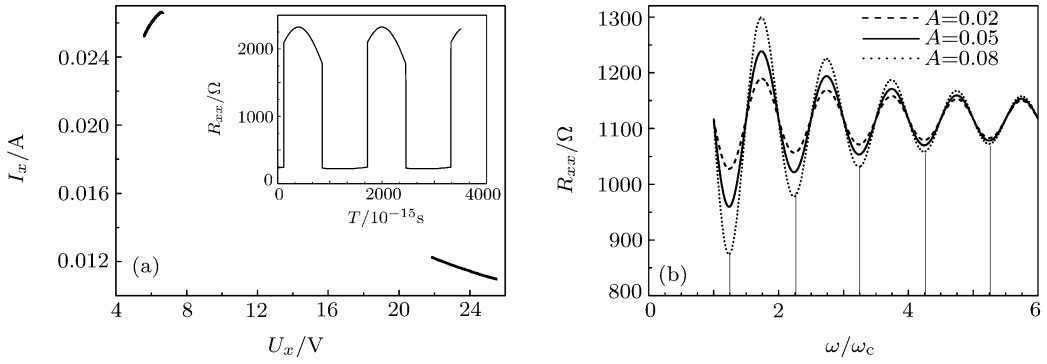


Fig.9. (a) The phase diagram of current–voltage. Only two nearly time-independent states exist, the inset is the resistance oscillations versus the time. (b) The resistance oscillations against ω/ω_c for different amplitude of MW. The local minimum resistance values can be obtained at ω/ω_c=integer+1/4.

4. Conclusions

We showed that real-space charge carriers transfer and delayed dielectric relaxation of the interface potential barrier could generate a NDC response in the GaAs/Al_xGa_{1-x}As heterostructure under a transverse magnetic field and MW radiations. For a small magnetic field (a small Hall angle), a dynamical perturbation or the MW radiation changes the stability of the NDC states and leads to bifurcations. The routes from period-doubling to chaos are revealed. For a large magnetic field, the system behaves as a bistable one, and the steady states are almost time-independent stable states. As a result, a positive constant resistance state is expected. Interestingly, the positive resistance shows a periodic oscillation with variable periodicity depending on the MW radiation frequency, as suggested by Andreev and co-workers.[27]

References

[1] Tsui D C, Stormer H and Gosssard A 1982 *Phys. Rev.* B **25** 1405

[2] Liu L, Liu J J and Zhang H 2007 *Acta Phys. Sin.* **56** 487 (in Chinese)

[3] Deng C S, Liu X L, Ma S S, Song Z Q and Xu H 2006 *Acta Phys. Sin.* **55** 2492 (in Chinese)

[4] Shangguan W Z, Xu J and Zhan S C 2005 *Chin. Phys.* **14** 2093

[5] Aoki K, Matsuura A and Takahashi Y 1994 *Semicond. Sci. Technol.* **9** 607

[6] Tzeng T S Y and Tzeng Y 2004 *Phys. Rev.* B **70** 085208

[7] Li G H, Xu D M and Zhou S P 2001 *Acta Phys. Sin.* **50** 1567 (in Chinese)

[8] Eberle W, Hirschinger J, Margull U and Prettl W 1996 *Appl. Phys. Lett.* **68** 3329

[9] Tzeng S Y T and Cheng Y C 2005 *Phys. Rev.* B **72** 205201

[10] Mani R G, Smet J H, von Klitzing K, Narayanamurti V, Johnson W B and Umansky V 2002 *Nature* (London) **420** 646

[11] Zudov M A, Du R R, Pfeiffer L N and West K W 2003 *Phys. Rev. Lett.* **90** 046807

[12] Yang C L, Zudov M A, Knuuttila T A, Du R R, Pfeiffer L N and West K W 2003 *Phys. Rev. Lett.* **91** 096803

[13] Studenikin S A, Potemski M, Coleridge P T, Sachrajda A and Wasilewski Z R 2004 *Solid State Commun.* **129** 341

[14] Ryzhii V and Vyurkov V 2003 *Phys. Rev.* B **68** 165406

[15] Vavilov M G and Aleiner I L 2004 *Phys. Rev.* B **69** 035303

[16] Iñarrea1 J and Platero G 2005 *Phys. Rev. Lett.* **94** 016806

[17] Koulakov A A and Raikh M E 2003 *Phys. Rev.* B **68** 115324

[18] Shi J and Xie X C 2003 *Phys. Rev. Lett.* **91** 086801

[19] Rivera P H and Schulz P A 2004 *Phys. Rev.* B **70** 075314

[20] Simovic B, Ellenberger C, Tranitz H P and Wegscheider W 2004 *Phys. Rev.* B **71** 233303

[21] Ryzhii V 2003 *Phys. Rev.* B **68** 93402

[22] Durst A C, Sachdev S, Read N and Girvin S M 2003 *Phys. Rev. Lett.* **91** 086803

[23] Lei X L and Liu S Y 2003 *Phys. Rev. Lett.* **91** 226805

[24] Lei X L 2004 *J. Phys.*: *Condens. Matter* **16** 4045

[25] Lü Y L, Xu D M and Zhou S P 2000 *Acta Phys. Sin.* 2000 **49** 1394 (in Chinese)

[26] Ng T K and Dai L X 2005 *Phys. Rev.* B **72** 235333

[27] Andreev A V, Aleiner I L and Millis A J 2003 *Phys. Rev. Lett.* **91** 056803

[28] Bergeret F S, Huckestein B and Volkov A F 2003 *Phys. Rev.* B **67** 241303

[29] Volkov A F and Pavlovskii V V 2004 *Phys. Rev.* B **70** 075314

[30] Schöll E and Aoki K 1991 *Appl. Phys. Lett.* **58** 1277

[31] Glisson T H, Hauser J R, Littlejohn M A, Hess K, Streetman B G and Shichijo H 1980 *J. Appl. Phys.* **51** 5445

[32] Hüpper G and Schöll E 1991 *Phys. Rev. Lett.* **66** 2372

[33] Schöll E 2001 *Nonlinear Spatio-Temporal Dynamics and Chaos in Semiconductors* (Cambridge: Cambridge University Press) p2

[34] Brennan K F and Park D H 1989 *J. Appl. Phys.* **65** 1156

[35] Lisheng Y 1990 *The Physics of Semiconductor Heterojunction* (Beijing: Science Press) pp5–108 (in Chinese)